

University of Massachusetts Amherst

From the Selected Works of William MacKnight

1980

Small-Angle X-Ray Scattering Study of Ionomer Deformation

William MacKnight, *University of Massachusetts Amherst*

E. J. Roche

R. S. Stein

T. P. Russell



Available at: https://works.bepress.com/william_macknight/243/



Small-Angle X-Ray Scattering Study of Ionomer Deformation

E. J. ROCHE,* R. S. STEIN,† T. P. RUSSELL,‡ and
W. J. MACKNIGHT, *Polymer Research Institute, Polymer Science and
Engineering Department and Materials Research Laboratory, University of
Massachusetts, Amherst, Massachusetts 01003*

Synopsis

The small-angle x-ray scattering (SAXS) pattern from a cesium salt of a 6.1 mole % ethylene-methacrylic acid (E-MAA) copolymer is shown to become azimuthally dependent on sample elongation. SAXS was measured using the Oak Ridge National Laboratory (ORNL) spectrometer with pinhole collimation and a two-dimensional position-sensitive detector. The sample was quenched prior to deformation to avoid crystallization of the ethylene unit which would complicate the interpretation of scattering. The observed SAXS patterns are interpreted in terms of several proposed models for the structure of ionomers. A model in which ionic aggregates are arranged on a paracrystalline lattice is found to be largely in disagreement with the results for undeformed and deformed samples. Spherical and lamellar models incorporating local structure around a central ionic core are capable of predicting the observed SAXS for the undeformed sample. A model of ellipsoidal deformation of the spherical shell-core model fails to predict the correct azimuthal dependence of scattering. However, a deformation scheme involving rotation of the lamellar model is more satisfactory.

INTRODUCTION

The physical structure and properties of ionomers have been studied extensively in recent years. These studies have largely supported the idea that ionic groups in these copolymers aggregate to form microphase separated domains. The most direct evidence for ionic aggregation has come from SAXS studies which shows a scattering maximum corresponding to a Bragg spacing of 20–40 Å for the salt forms but not for the un-ionized copolymers.^{1–4} In ionomers formed by the neutralization of ethylene-methacrylic acid (E-MAA) copolymers the small-angle x-ray scattering (SAXS) maximum has been observed to persist to temperatures above the melting point of the ethylene units and to disappear on saturation with water.

Several different interpretations have been advanced for the cause of the SAXS maximum. Longworth and Vaughan¹ proposed that the peak represents a structural repeat distance within ionic domains. On the basis of an empirical rule for light scattering these authors suggested that at least five repeat periods must be present indicating a domain size of 150–200 Å. Subsequently, Cooper et al.⁴ proposed a model in which aggregates contain only up to seven or eight

* Present address: CEA-CEN Grenoble, DRF-G/Physique du Solide, Cedex 85, 38/Grenoble-Gare, France.

† To whom correspondence should be sent.

‡ Present address: Johannes-Gutenberg Universität, Institut für Physikalische Chemie der Universität Mainz, 6500 Mainz, Germany.

ion pairs and would thus have a radius of about 5 Å. The aggregates are arranged on a paracrystalline lattice with a spacing of 30–40 Å. The SAXS maximum for Cooper's model results from interaggregate interference rather than intraaggregate interference as in the model of Longworth and Vaughan. The paracrystalline lattice is considered to extend over the whole sample in Cooper's presentation. However, the possibility of a paracrystalline lattice extending over only portions of the sample might also be considered. MacKnight et al.³ proposed a shell-core model for ionomer aggregate structure in which a 3–13 Å ionic core is separated from a surrounding ionic shell by a distance corresponding approximately to the Bragg spacing. The shell-core structures are thought to be widely separated and randomly arranged within the sample. The SAXS maximum thus arises only from the intraaggregate shell-core interference and not from any interaggregate interference.

It should be noted that the shell-core model of MacKnight et al.³ is a dilute scattering model. This is in contrast to concentrated systems where the particle volume fraction is large enough so that a scattering maximum may arise from order imposed on the system by the effect of the excluded volume of the particles themselves. Riley and Oster⁵ showed, using a formulation by Fournet,⁶ that a particle volume fraction of about 33% is necessary for a maximum to arise from excluded volume effects. This is much larger than the particle volume fraction for ionomers which has been shown to be of the order of a few percent.^{3,7}

The observation of SAXS scattering during sample elongation is a possible means of testing these various models. Such measurements were made by Longworth and Vaughan¹ and also by MacKnight et al.³ on ionomers made from ethylene-methacrylic acid copolymers. Longworth and Vaughan reported no azimuthal variation in the ionomer SAXS peak even though orientation effects were observed in the SAXS maximum at lower angles assigned to the polyethylene lamellar spacing. Taggart⁸ et al. observed essentially no change in the ionomer SAXS peak with sample elongation in a study of the Na⁺ salt of a 3.8 mole % copolymer at elongation up to 70%. In both of these studies, substantial crystallinity of the ethylene units was present. This crystallinity could have greatly affected the deformation behavior of the samples. To characterize the deformation behavior of ionomers it is desirable to have noncrystalline samples in which the only morphological structures are the ionic aggregates. This has been accomplished in the current study by using samples with larger ionic concentrations, which may be quenched to avoid polyethylene crystallization. In addition, the deformation behavior has been studied up to elongation of 300% which may enhance the deformation effect. Finally, the SAXS pattern has been studied on the 10-m Oak Ridge National Laboratory (ORNL) SAXS camera with rotating anode generator using pinhole collimation and a position sensitive detector. This camera combines high source intensity and excellent detector sensitivity, which greatly increases the ease of detection over photographic methods. The use of pinhole collimation makes unnecessary the use of a slit-demeaning procedure which is difficult or impossible for anisotropic scattering systems.

SAXS OF IONOMER DEFORMATION

3

EXPERIMENTAL

An ethylene-methacrylic acid copolymer containing 6.1 mole % methacrylic acid units was obtained from the duPont Company. The number average and weight average molecular weights were characterized as 5400 and 25,500, respectively, using gel permeation chromatography with trichlorobenzene as solvent at 137°C. The melting point was measured as 93°C by differential scanning calorimetry. The copolymer was neutralized by dropwise addition of cesium methoxide to a 1% solution in filtered *p*-xylene at 137°C under nitrogen gas. Films were compression-molded at 110°C and then quenched in a dry ice-isopropanol mixture and then dried *in vacuo* at room temperature. The percent neutralization was measured to be 94% for a thin film using the infrared spectroscopic procedure of MacKnight et al.⁹ The x-ray linear absorption coefficient was measured to be 65.2 cm⁻¹ on the 0.036-cm-thick film used in subsequent scattering measurements. The mass density of the thin film was determined to be 1.12 g/cm³. The mass absorption coefficient of the film is then 58.2 cm²/g which corresponds to 85% ionization.

WAXS measurements showed the undeformed film to be amorphous. Measurements later made on the sample after elongation to 300% also showed only an amorphous peak but with an indication of amorphous orientation in the stretching direction.

SAXS measurements were made on the ORNL spectrometer using pinhole collimation and a two-dimensional position-sensitive detector recently described by Hendricks.¹⁰ The spectrometer uses a 6 kW Rigaku-Denki rotating anode generator, graphite crystal monochromator, and a monitor detector to measure incident beam intensity changes. The collimation system consists of two 1 mm pinholes separated by 5 m. The detector is a two-dimensional position-sensitive proportional with an active area of 20 × 20 cm developed by Borkowski and Kopp.¹¹ A 1.2-m sample-to-detector distance was used in this study which is the minimum currently available. Scattering data can be obtained up to $2\theta \approx 4^\circ$ using this distance with Cu K α radiation ($\lambda = 1.54 \text{ \AA}$).

Sample scattering curves and attenuation factors were measured at a series of elongations. Typical total scattering count values of several hundred to 1000 were obtained at each angular position giving a precision of 3-7%. A time of 3 to 4 hr was allowed to elapse between successive measurements at different elongations to allow for possible sample relaxation. Background scattering was measured in the absence of any sample, normalized according to the sample attenuation factor, and then subtracted from the scattering at each elongation.

RESULTS AND DISCUSSION

Scattering Curves

Figure 1 shows iso-intensity SAXS contours for a series of elongations from 0% to 300% with the stretching direction vertical. At elongations above ca. 60% the scattering becomes strongly azimuthally dependent. A distinct two-point pattern is observed at 300% elongation. Figure 2 shows scattering curves at 0% and 300% elongation. The curve for the underformed sample has been obtained by a circular averaging about the incident beam position. The resulting curve is very similar to those previously observed for these ionomers.¹⁻⁴ The peak

(F1)

(F2)

Fig. 1. Isointensity SAXS contours of cesium salt of E-MMA at various deformations: (a) 0%; (b) 9%; (c) 30%; (d) 35%; (e) 45%; (f) 60%; (g) 100%; (h) 300%.

corresponds to a Bragg spacing of 34 Å. A significant zero-order scattering component is observed in the range of $2\theta < 1^\circ$. At 300% elongation curves have been obtained at 0° and 90° azimuthal angles (ϕ) to the stretching directions by averaging points on opposite sides of the incident beam for detector wires lying in the appropriate directions. The scattering peak at $\phi = 90^\circ$ is greatly intensified over that of the undeformed sample while no peak is observed at $\phi = 0^\circ$.

SAXS OF IONOMER DEFORMATION

5

Figure 3 shows the data at $\phi = 0^\circ$ and 90° for a series of elongations after normalizing for changes in sample thickness and attenuation factor. The scattering peak at $\phi = 0^\circ$ is seen to shift to lower angles and decrease in intensity up to about 45% elongation and then to disappear at higher elongations. The maximum increases in intensity but changes little in position at $\phi = 90^\circ$. The observed Bragg spacings are compared in Figure 4 to the prediction for an affine deformation. For the affine case, the following relations hold:

$$d_{\parallel} = \lambda d_0 \quad (1)$$

$$d_{\perp} = \lambda^{-1/2} d_0 \quad (2)$$

where λ is the ratio of the length of the sample between clamps after deformation to the length before deformation, d_{\parallel} is the spacing at 0° azimuthal angle, and d_{\perp} is the spacing at $\phi = 90^\circ$. No points are shown for deformation above $\lambda = 1.6$ at $\phi = 0^\circ$ since no SAXS maximum is observed. Error bars indicate the maximum and minimum peak position that might have been obtained allowing for the possible statistical errors in counting. The observed peak shifts are seen to disagree with the affine model, particularly since no peak shift is observed at $\phi = 90^\circ$.

Fig. 3. (a) SAXS intensity profiles at $\phi = 0^\circ$ for E-MMA cesium salt at $\lambda = 1.0$ (O); 1.3 (Δ); 1.45 (\square); 2.0 (∇); 4.0 (\bullet). (b) SAXS intensity profiles at $\phi = 90^\circ$ for E-MMA cesium salt at $\lambda = 1.0$ (O); 1.3 (Δ), 1.45 (\square); 2.0 (∇); 4.0 (\bullet).

Fig. 3. (Continued from previous page).

Comparison with Predictions of Scattering Models

Paracrystalline Lattice Model

In this model proposed for ionomers by Marx et al.⁴ the ionic aggregates are assumed to be arranged on a disordered lattice with the lattice spacing nearly equal to the observed Bragg spacing of the ionic maximum. The intensity of scattering as formulated by Hosemann and Bagehi¹² is given by

$$I(s) = (\overline{F^2} - \overline{F}^2) + (\overline{F^2}/v)Z[S]^{-2} \quad (3)$$

6 pt #

change to $\overline{F^2}$ ok change top layer
(line on top shall be extended further)

Fig. 4. Bragg spacings calculated at $\phi = 0^\circ$ (O) and $\phi = 90^\circ$ (Δ) as a function of extension ratio. The dotted line is the spacing predicted for affine deformation.

long

SAXS OF IONOMER DEFORMATION

where $s = 2(\sin\theta)/\lambda$, F is the structure factor for the points in the lattice, and v is the volume of a lattice cell. $Z(s)$ is the interference factor which, for the case of disorder of the second kind for an n -dimensional lattice is given by

$$Z(s) = \prod_{k=1}^n \frac{1 - |b_K|^2}{(1 - |b_K|)^2 + 4|b_K| \sin^2(\pi a_K |s| \sin\psi)} \quad (4)$$

where a_K is the lattice spacing in the K th direction, and ψ is the angle between this direction and the scattering vector s . The function b_K characterizes the extent of disorder in the K th direction and is given by

$$b_K = \exp(-2\pi^2 s^2 D_K^2) \quad (5)$$

where D is a disorder parameter with unity of a in eq. (3). Here S is the shape factor of the lattice as a whole, the so called "brick factor." V is the volume of a lattice cell.

In the treatment of Marx et al.⁴ the lattice is assumed to extend over the entire sample. In this case of an essentially infinite lattice, the shape factor S corresponds to a delta function at zero scattering angle and thus in practice no zero-order scattering is predicted. These authors have indicated an ionic aggregate size of two to seven ion pairs is fairly consistent with such a model, a size which corresponds to a particle radius of about 5 Å. This value is assumed here. The fluctuation term $\overline{F^2} - F^2$ gives an angularly independent scattering. The intensity observed at large angles is assumed to be equal to this term. The point structure-factor F is assumed to be represented by the sphere shape-factor given by

change to capital S

change to $\overline{F^2}$

$$F = 3V_s [(\sin hR - hR \cos hR)/(hR)^3] \quad (6)$$

where $h = 2\pi s$, R is the sphere radius, and V_s is the sphere volume.

To compare the predicted angular dependence of scattering to that observed experimentally, only the angularly dependent terms in eq. (3) need be considered. A normalization factor is then adjusted so that the sum of intensity points for the model and experimental curves are equal. A relative error of the model fit δ can then be defined as

$$\delta = \sum_j |(I_M)_j - (I_E)_j| / \sum_j (I_E)_j \quad (7)$$

where I_M and I_E are the individual model and experimental intensities at a given scattering angle.

Figure 5 shows a comparison at the calculated curve for an infinite paracrystalline model and the experimental curve for the undeformed sample. For the model curve a lattice spacing of 34 Å has been used along with a disorder parameter D of 6 Å which corresponds to the best obtainable fit. The large deviation of 0.7 for δ results because the model gives no source of zero-order scattering while a strong zero-order component is experimentally observed. An important point in this regard is that the zero-order scattering observed in ionomers at $2\theta < 1^\circ$ is much greater than that seen for the corresponding acid samples. Thus, this scattering results from structures present only in the salt form and not from foreign heterogeneities that would be present in both acid and salt samples.

F5

A finite paracrystalline lattice can exhibit zero-order scattering and might be

Fig. 5. Infinite paracrystalline lattice model (—) fit to experimental data (O) ($A = 3.4$ nm; $R_p = 0.5$ nm, $D = 1.2$ and 2.0 nm).

expected to better fit the experimental data. Hosemann et al.¹³ have recently shown that at low angles the zero-order scattering component can be analyzed by using the relation

$$Z|S|^2 = \left(\frac{2b_1}{1+b_1} \right) \left(\frac{2b_2}{1+b_2} \right) \left(\frac{2b_3}{1+b_3} \right) |S|^2 \quad (8)$$

Here a cubic lattice is assumed with $(N + 1)$ lattice points in each of the three perpendicular directions. The shape factor S is in this case given by

$$S = \left(\frac{\sin \pi N h_1}{\pi h_1} \right) \left(\frac{\sin \pi N h_2}{\pi h_2} \right) \left(\frac{\sin \pi N h_3}{\pi h_3} \right) \quad (9)$$

where $h_K = a_K s$.

The best fit of the zero-order scattering in terms of eq. (9) is given in Figure 6 for which values of 34 \AA for a_K , 10 \AA for D_K , and a value of 1 for N have been used to obtain an error δ of 0.05. For larger values of N a large discrepancy between the experimental and calculated curves is found irrespective of the value of the disorder parameter. The analysis indicates that only a finite paracrystalline model of very limited extent can possibly explain the observed scattering.

The use of a paracrystalline model with a large lattice size is also questionable in view of the observed deformation behavior found in this study. An infinite paracrystalline model would be expected to show peak shifts similar to the affine

(46)

Fig. 6. Finite paracrystalline lattice model (—) fit to experimental data (O) ($A = 2.5$ nm; $R_{LATT} = 7.5$ nm; $R_p = 0.5$ nm; $D = 1.8$ nm; $\Delta\rho = 1.0$; $\delta = 7.6\%$).

deformation model. Thus both the existence of the observed zero-order scattering and the highly nonaffine nature of the deformation argue that if a paracrystalline model is to be used it must have an overall lattice of a very limited size.

Local Structural Models

The requirement of zero-order scattering and the observed deformation behavior suggest that models involving short-range order or local structure are more appropriate for ionomers. Such structures can be expected to exhibit strains in the region of the ionic structure which are quite different from the overall strain patterns of the sample as a whole. The finite size of these structures will give rise to the necessary zero-order scattering component.

Spherical core-shell model. Figure 7 shows a schematic version of the model originally proposed by MacKnight et al.³ consisting of a spherical ion-rich core with a shell of associated ions. A general representation of this model might assign different electron density values to the region outside of the shell, the shell, the inter-shell-core region, and the ion core. In this treatment it is assumed that the electron density of the region outside of the shell and the inter shell-core region are the same. The shape function for such a model can be represented by

$$S(\mathbf{r}) = \begin{cases} \rho_1, & 0 \leq r \leq R_1 \\ 0, & R_1 < r \leq R_2 \\ \rho_3, & R_2 < r \leq R_3 \\ 0, & R_3 < r \end{cases} \quad (10)$$

F7

Fig. 7. Shell-core model of MacKnight et al. (ref. 3).

where R_1 is the core radius and R_2 and R_3 are the inner and outer shell radii. The electron densities ρ_1 and ρ_3 are given by

$$\begin{aligned}\rho_1 &= \rho'_1 - \rho'_3 \\ \rho_3 &= \rho'_2 - \rho'_3\end{aligned}\quad (11)$$

where ρ'_1 , ρ'_2 , and ρ'_3 are the electron densities of the core, shell, and the inter-shell-core region, respectively. The scattering from this model is represented by

$$\frac{F}{\rho_1} = \frac{3[\sin(hR_1) - hR_1 \cos(hR_1)]}{h^3[R_1^3 - A(R_2^3 + R_3^3)]} + \frac{3A[\sin(hR_3) - hR_3 \cos(hR_3) - \sin(hR_2) + hR_2 \cos(hR_2)]}{h^3[R_1^3 - A(R_2^3 + R_3^3)]} \quad (12)$$

where $A = \rho_3/\rho_1$. A fit of the experimental curve with an error of 7% was achieved with $R_1 = 5 \text{ \AA}$, $R_2 = 41 \text{ \AA}$, $R_3 = 46 \text{ \AA}$, and a value for A of 0.007.

Various mechanisms might be considered for the deformation of this model. One example mechanism is considered here in which the shell and core structures are elliptically deformed in the direction of stretching. Since no change in the Bragg spacing at $\phi = 90^\circ$ is observed experimentally the shell and core dimensions along that direction will be assumed to be constant. The relative changes in intensity and peak shift at $\phi = 0^\circ$ are then compared to the experimental curves to test the validity of the mechanism.

The dimensions of the ellipsoid parallel to the stretching direction change according to

$$\begin{aligned}(R_1) &= \nu_1(R_1)_0 \\ (R_2) &= \nu_2(R_2)_0 \\ (R_3) &= (R_3)_0 + (\nu_2 - 1)(R_2)_0\end{aligned}\quad (13)$$

while A is assumed to vary as

$$A' = A(V_s V'_c / V'_s V_c) \quad (14)$$

where V_s and V_c are the shell and core volumes and primed variables denote values after deformation. The structure factor F_E for ellipsoids has been discussed by Barber.¹⁴ For the case of ellipsoids arranged according to the scattering direction,

$$F_E = [(3/U^3)(\sin U - U \cos U)]^2 \quad (15)$$

SAXS OF IONOMER DEFORMATION

where

$$U = (4\pi/\lambda) a \sin(\theta/2) \{ \cos^2(\theta/2) \cos^2\phi + (b^2/a^2) [1 - \cos^2(\theta/2) \cos^2\phi] \}^{1/2} \quad (16)$$
 where a and b are the long and short axes of the ellipsoid, respectively, and ϕ is the azimuthal angle. Figures 8 and 9 show illustrative curves calculated for a relatively small deformation of the core compared to the shell. The scattered intensity at $\phi = 0^\circ$ decreases with increasing ellipsoid eccentricity as in the experimental plot but a decreased intensity is also observed for $\phi = 90^\circ$, contrary to the experiment. Deformation schemes in which the core is deformed more than the shell give a less rapid decrease in intensity at $\phi = 90^\circ$ compared to $\phi = 0^\circ$ but are still much different than the experimental results.

6pt #
 F8+9

Lamellar models. It is known that salts of lipids (fatty acids) can form lamellar micelles in either polar or nonpolar media. This suggests¹⁵ that lamellar structures might also be present in ionomers. The scattering from layered structures has been treated by several authors.^{13,16,17} In most cases the layers have lateral dimensions large compared to the innerlayer spacing, allowing the use of the Hosemann¹² s^2 factor to reduce the scattering from the three-dimensional model. For ionomers the lateral dimension of the layers is likely to be comparable to the interlayer spacing as evidenced by the relatively small overall particle radius of gyration. Thus it is really necessary to calculate the entire scattering considering the three-dimensional nature of the layers. In this work only a two-dimensional model is used for reasons largely of mathematical simplicity. It is felt that this two-dimensional calculation is sufficient to assess the potential of a lamellar model for ionomers.

A model with two parallel ion-rich layers was initially examined but failed to

Fig. 8. Predicted SAXS profiles for the deformed shell core model at $\phi = 0$. (●) $\nu_1 = 1, \nu_2 = 1$; (Δ) $\nu_1 = 1.02, \nu_2 = 1.2$; (○) $\nu_1 = 1.04, \nu_2 = 1.4$; (▽) $\nu_1 = 1.06, \nu_2 = 1.6$.

Fig. 9. Predicted SAXS profiles for the deformed shell-core model at $\phi = 90^\circ$. Symbols defined in Figure 8.

yield a sufficient scattering maximum. The three-layer model shown in Figure 10, where the thicknesses of the inner and outer layers are assumed to both equal L , was adopted for simplicity. It is also assumed that the matrix and interlayer regions (L_2) have the same electron densities. The shape function for this model is given by

$$S(\mathbf{x}) = \begin{cases} \rho_1 & \begin{cases} |x_1| \leq L_1/2 \\ |x_2| \leq W/2 \end{cases} \\ \rho_2 & \begin{cases} L_1/2 + L_2 \leq |x_1| \leq 3L_1/2 + L_2 \\ |x_2| \leq W/2 \end{cases} \\ 0, & \text{all other } x \end{cases} \quad (17)$$

*Graphical
 must
 large
 trace
 as shown*

where W is the lamellar width and $|x_1|$ and $|x_2|$ denote the absolute value of the magnitude of the vector \mathbf{x} in the direction perpendicular and parallel to the layer direction, respectively. The structure factor F for this model is different for different values of μ as shown in Figure 10. It is given by (a) $\mu > \mu_3$,

$$F = \left[\frac{\sin(\pi s_1 L_1)}{\pi s_1} + A \left(\frac{\sin[\pi s_1(3L_1 + L_2)]}{\pi s_1} - \frac{\sin(\pi s_1(L_1 + 2L_2))}{\pi s_1} \right) \right] \times \frac{\sin(\pi s_2 W)}{\pi s_2} \quad (18)$$

6pt #

Equation (18) applies only for $\mu > \mu_2$, as shown in Figure 10. For $\mu < \mu_3$, we have (b) $\mu < \mu_2$,

$$F = \frac{\sin(\pi s_1 L_1)}{\pi s_1} \frac{\sin(\pi s_2 W)}{\pi s_2} \quad (19)$$

Fig. 10. Schematic representation of the lamellar model.

(c) $\mu_2 \leq \mu \leq \mu_3$,

$$F = \left(\frac{\sin(\pi s_1 L_1)}{\pi s_1} + A \left(\frac{\sin(\pi s_1 x')}{\pi s_1} - \frac{\sin(\pi s_1 (L_1 + 2L_2))}{\pi s_1} \right) \right) \frac{\sin(\pi s_2 W)}{\pi s_2} \quad (20)$$

where $x' = (W/2) \tan \mu - L_1/2 - L_2$, s_1 and s_2 denote the magnitudes of the components of \mathbf{s} in the 1 and 2 directions, and $A = \rho_2/\rho_1$.

The structure factor for an individual lamellar structure depends on the Bragg scattering angle θ and the azimuthal angle μ for that structure. The angle μ is related to the macroscopic azimuthal angle relative to the stretching direction ϕ and the tilt angle ω between the stretching direction and the direction perpendicular to the layers by

$$\mu = \phi - \omega \quad (21)$$

The magnitude of \mathbf{s} in the 1 and 2 directions is given by

$$\begin{aligned} |\mathbf{s}_1| &= s_1 \sin \mu \\ |\mathbf{s}_2| &= s_2 \cos \mu \end{aligned} \quad (22)$$

A Gaussian distribution of tilt angles is assumed

$$g(\omega) = C \exp \left[-(\omega^2/\beta^2) \right] \quad (23)$$

where β is the distribution width, and C is the normalization constant. The convention is used that $\omega = 0$ for a layer lying parallel to the stretching direction. In the undeformed state the distribution of ω is random corresponding to large β . The distribution of layer orientation can be characterized by a two-dimensional orientation function

$$f(\omega) = 2 \langle \cos^2 \omega \rangle_{av} - 1 \quad (24)$$

for random layer orientation, $f(\omega)$ is 0. For the case with all layers parallel to the stretching direction, $f(\omega)$ is unity.

A fit of the experimental data for the undeformed sample was made assuming random layer orientation. For values of $L_1 = 6 \text{ \AA}$, $L_2 = 28 \text{ \AA}$, $w = 20 \text{ \AA}$, and $A = 0.2$ an error of 6% was obtained.

Figure 11 shows scattering curves at $\phi = 0^\circ$ for values of $f(\omega)$ corresponding to increasing orientation of the layers along the stretching direction. Figure 12 shows the corresponding curves at $\phi = 90^\circ$. The model is observed to correctly predict decreased intensities at $\phi = 90^\circ$. A discrepancy between the model and experiment exists in that the model predicts the peak shift at $\phi = 0^\circ$ to occur at a slow rate with respect to the intensity decrease.

This discrepancy might be avoided by a three-dimensional lamellar model or by considering the possibility of stretching, i.e., changes in L_1 or L_2 with deformation. The calculations do indicate that a lamellar model has a good potential for explaining the undeformed and deformed scattering curves.

Other local-structure models incorporating a combination of rotation and stretching of ellipsoids or incomplete ellipsoids might also be considered. The deformation schemes considered in this work can only be regarded as examples involving a single mechanism and structure. The real case is undoubtedly more complex.

F11
F12

Fig. 11. Predicted SAXS profiles at $\phi = 0^\circ$ for lamellar model with $L_1 = 0.8 \text{ nm}$, $L_2 = 2.6 \text{ nm}$, $W = 6.0 \text{ nm}$, and $A = 0.2$. The different profiles correspond to $f = 0$ (\blacktriangle); 0.5 (\triangle); 0.67 (\bullet) and 0.89 (\circ).

SAXS OF IONOMER DEFORMATION

Fig. 12. Predicted SAXS profiles at $\phi = 90^\circ$ for lamellar model with $L_1 = 0.8$ nm, $L_2 = 2.6$ nm, $W = 6.0$ nm, and $A = 0.2$. Symbols are defined in Figure 11.

CONCLUSIONS

The scattering curves from the cesium salt of an ethylene-methacrylic acid copolymer have been obtained in the undeformed state and also at various elongations. The absence of any significant crystallinity of the ethylene units has allowed an interpretation of scattering solely in terms of ionic aggregate structures. A marked azimuthal dependence of scattering is observed for sample elongation of 60% or more. The Bragg spacings at azimuthal angles parallel and perpendicular to the stretching direction vary in a manner which is very dissimilar to predictions from affine deformation. This indicates that dimensions between ionic structures giving rise to the interference maximum are changing very differently than the dimensions of the sample as a whole.

An infinite paracrystalline lattice model fails to explain the data for the undeformed sample since it contains no origin of zero-order scattering. A finite paracrystalline lattice model gives a better fit to experiment for a lattice having on the order of eight points. However, this model must be questioned since this small lattice can no longer be correctly described by the paracrystalline lattice statistics. Paracrystalline lattice models would be expected to exhibit changes in peak spacings similar to the affine case, which is contrary to experiment, although a finite model could possibly deform to a lesser degree than the matrix.

The observed zero-order scattering component and the deviation from affine behavior suggest that models involving local structure are more appropriate. A spherical shell-core model and a two-dimensional lamellar model involving short-range structure are capable of explaining the data for the undeformed

sample. An ellipsoidal deformation scheme of the shell-core model failed to give an intensity increase at $\phi = 90^\circ$, which was observed experimentally. A layer rotation-deformation scheme for the lamella model correctly predicts the intensity observed at $\phi = 90^\circ$ and the decrease at $\phi = 0^\circ$ but does not correctly explain the peak shift at $\phi = 0^\circ$. An extension of the model to three dimensions or a consideration of stretching or an additional deformation mechanism might give more complete correspondence with experiment.

We are grateful to the National Science Foundation, the Army Research Office (Durham), and the Materials Research Laboratory of the University of Massachusetts. We are greatly indebted to Dr. Robert W. Hendricks of Oak Ridge National Laboratories for use of his SAXS facilities and for assistance with the scattering experiments. One of us (T.P.R.) is grateful to the Oak Ridge Associated Universities for their financial assistance during the course of the experiments.

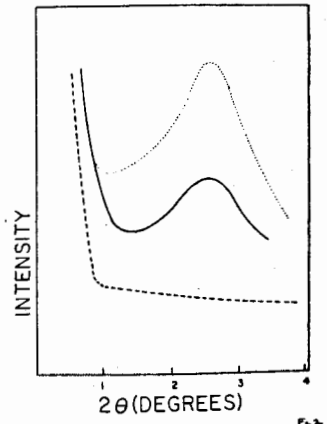
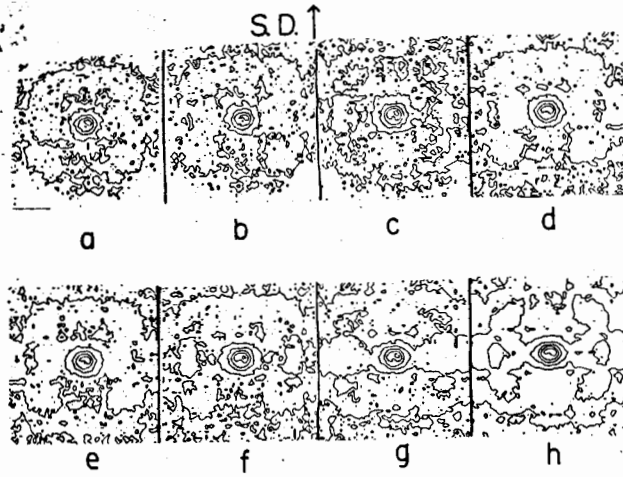
References

1. R. Longworth and D. J. Vaughan, *Nature (London)*, **2**(18), 85 (1968).
2. R. Longworth, in *Ionic Polymers*, L. Holliday, Ed., Applied Science, New York, 1975, [Chap. 2].
3. W. J. MacKnight, W. P. Taggart, and R. S. Stein, *J. Polym. Sci. Polym. Symp.*, **45**, 113 (1974).
4. C. L. Marx, D. F. Caulfield, and S. L. Cooper, *Macromolecules*, **6**, 3 (1973); **6**, 334 (1973).
5. D. Riley and G. Oster, *Discuss. Faraday Soc.*, **11**, 107 (1951).
6. G. Fournet, *C. R. Acad. Sci.*, **228**, 1421 (1949).
7. E. Roche, Ph.D. thesis, University of Massachusetts, 1978.
8. W. P. Taggart, Ph.D. thesis, University of Massachusetts, 1973.
9. W. J. MacKnight, L. W. McKenna, B. E. Read, and R. S. Stein, *J. Phys. Chem.*, **72**, 1122 (1968).
10. R. W. Hendricks, *J. Appl. Crystallogr.*, **11**, 15 (1978).
11. C. J. Borkowski and M. K. Koop, *Rev. Sci. Instrum.*, **39**, 1515 (1968).
12. R. Hosemann and S. N. Bagchi, *Direct Analysis of Diffraction by Matter*, North-Holland, Amsterdam, 1962, Chap. 3.
13. R. Hosemann, R. Loboda-Čačkovič, and D. Weick, "Small Angle X-Ray Scattering of Fibrous Microparacrystals," to be published.
14. P. W. Barber and D. Wang, *Appl. Opt.*, **17**(5), 797 (1978).
15. W. J. MacKnight, *Polym. Prepr. Am. Chem. Soc. Div. Polym. Chem.*, **11**, 504 (1970).
16. G. Porod, *Z. Naturforsch. Teil A*, **4**, 401 (1949).
17. O. Kratky and G. Porod, *J. Colloid Sci.*, **4**, 35 (1970).

Received March 5, 1979

Accepted January 11, 1980

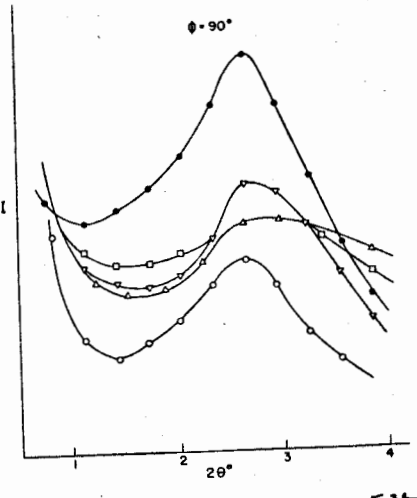
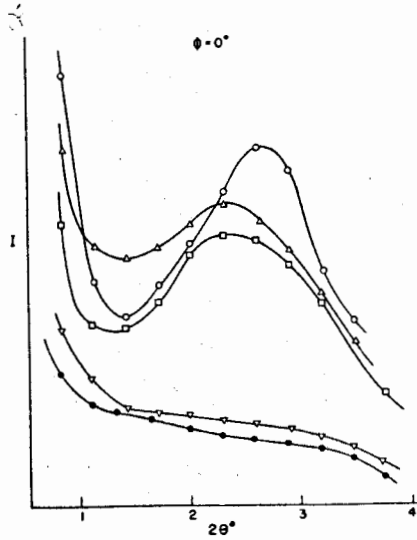
break



303
JRL *Phys* ISSUE *KB 9* FIG 1
50 % OF ORIG ——— DENSITOMETER

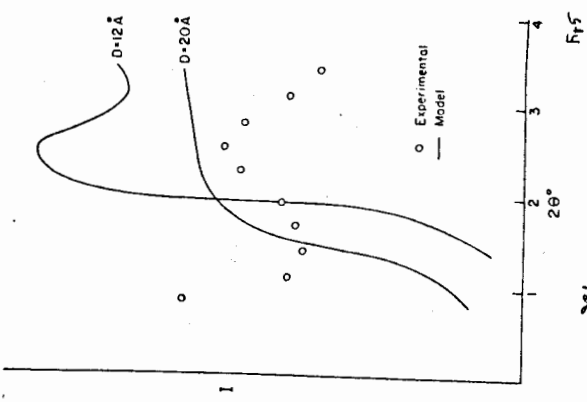
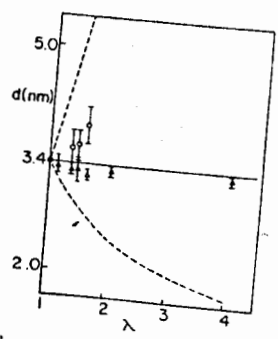
Fig 1

303
JRL *Phys* ISSUE *KB 9* FIG 2
30 % OF ORIG ——— DENSITOMETER



303
JRL *Phys* ISSUE *KB 9* FIG 3A
40 % OF ORIG ——— DENSITOMETER

303
JRL *Phys* ISSUE *KB 9* FIG 3B
40 % OF ORIG ——— DENSITOMETER



303
JRL *Phys* ISSUE *KB 9* FIG 4
40 % OF ORIG ——— DENSITOMETER

303
JRL *Phys* ISSUE *KB 9* FIG 5
40 % OF ORIG ——— DENSITOMETER

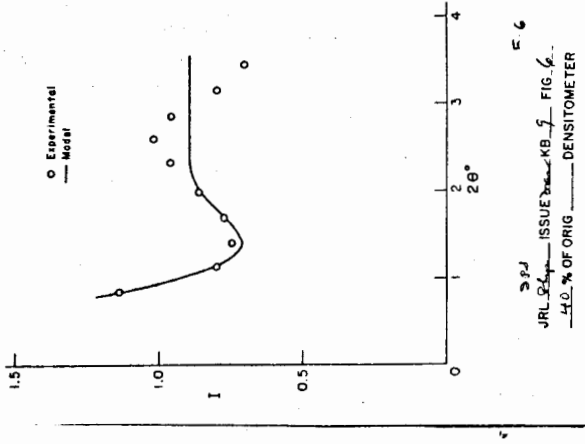


Fig 6
JRL 8249 ISSUE KB 7 FIG 6
40% OF ORIG DENSITOMETER

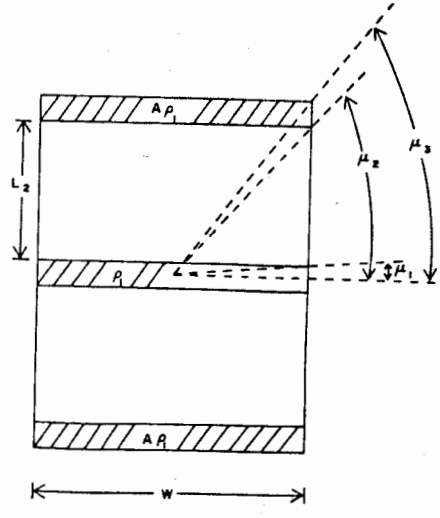


Fig 10
JRL 8249 ISSUE KB 9 FIG 10
40% OF ORIG DENSITOMETER

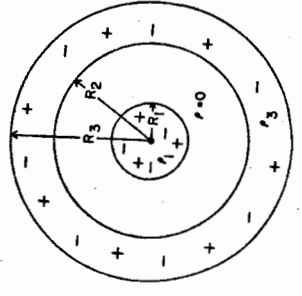


Fig 7
JRL 8249 ISSUE KB 7 FIG 7
40% OF ORIG DENSITOMETER

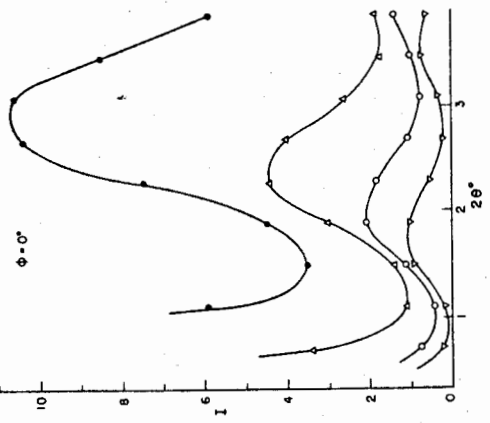


Fig 8
JRL 8249 ISSUE KB 9 FIG 8
40% OF ORIG DENSITOMETER

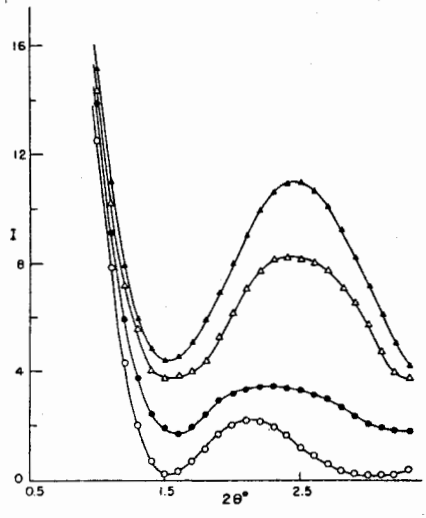


Fig 11
JRL 8249 ISSUE KB 9 FIG 11
40% OF ORIG DENSITOMETER

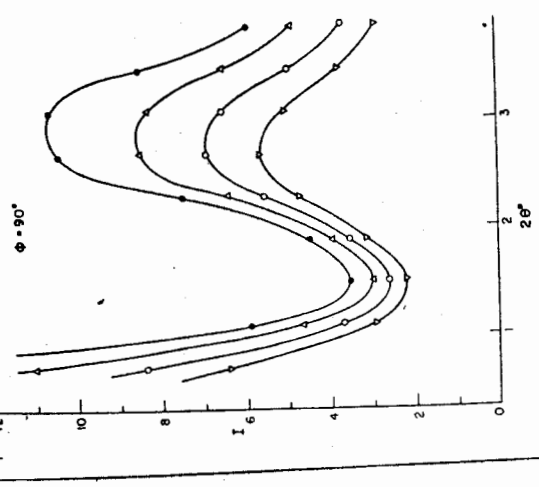


Fig 9
JRL 8249 ISSUE KB 9 FIG 9
40% OF ORIG DENSITOMETER

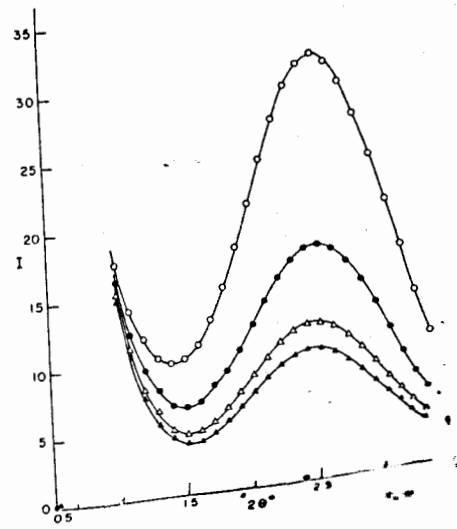


Fig 12